3rd May

Griebel, A., Bennett, L. T., Culvenor, D. S., Newnham, G. J., & Arndt, S. K. (2015). Reliability and limitations of a novel terrestrial laser scanner for daily monitoring of forest canopy dynamics. *Remote Sensing of Environment*, *166*, 205-213.

2.2. Instrument description

The VEGNET scanner (CSIRO, Australia) is a simplified and low-cost version of existing terrestrial laser scanners like Riegl VZ-400 (Calders et al., 2015), FARO Photon 120 (Pueschel, Newnham, & Hill, 2014), Leica C10 (Hancock et al., 2014) or Echidna (Zhao et al., 2013), and was designed for automated daily monitoring of crown structural dynamics rather than extracting detailed measures of forest structure at any one point in time. The sensor head consists of an inclined 45° prism that fixes the scan angle to 57.5° zenith (hinge angle, Jupp et al., 2009). The prism rotates through 360° azimuth during a complete scan. The class 2 red laser (635 nm, 0.6 mrad beam divergence) has an effective range of 60 m for green foliage, making it suitable for monitoring the structure of forests with canopy heights up to approximately 30 m. Distance to canopy objects is measured using phase-based range-finding, whereby range is inferred from the phase shift between transmitted and reflected laser energy modulated at a known frequency (Culvenor et al., 2014, Pueschel et al., 2014). The chance of multiple hits is minimised by the very low beam divergence, but partial and multiple hits can be visually observed in the canopy. Night-time operation is required due to the wavelength of the range finder to produce reliable range estimates of up to 60 m. The slow sample rate of the range finder (2–0.25 Hz) does not allow visually distinguishing the exact target, but the largest uncertainty with range recordings is assumed to be in the upper canopy consisting mainly of leaves and small branches that are most likely affected by wind.

Continuous LIDAR system?

2nd May

Eitel, J. U., Vierling, L. A., & Magney, T. S. (2013). A lightweight, low cost autonomously operating terrestrial laser scanner for quantifying and monitoring ecosystem structural dynamics. *Agricultural and forest meteorology*, *180*, 86-96.

Table 1. Approximate costs for ATLS as of 2013 (in U.S. dollars).

Item	Provider	Date quoted	Qty	Amount (USD)
ILR1191 laser distance sensor	Micro-Epsilon Messtechnik GmbH & Co. KG, 94496 Ortenburg, Germany	1/20/2012	1	$5575
PTU-46–17W pan tilt unit	FLIR Motion Control Systems, Inc., Burlingame, CA 94010, USA	1/20/2012	1	$2765
CST/Berger "Value Line" Tribrach	Tiger Supplies Inc., 27 Selvage St., Irvington NJ 07111, USA	4/20/2012	1	$100
Seco Fixed Tribrach Adapter	Tiger Supplies Inc., 27 Selvage St., Irvington NJ 07111, USA	4/20/2012	1	$33
CR1000 datalogger	Campbell Scientific, 815 West 1800 North, Logan, UT 84321-1784, USA	1/19/2012	1	$1383
NL115 Ethernet Interface & CompactFlash Module for datalogger			1	$274
2G CompactFlash Memory Card			1	$87
PC400 datalogger support software (includes CRBasic programming language)			1	$303
Power supply (battery, 70W solar panel, Morning Star SunSaver-10 10A 12V Regulator)			1	$1221
Custom laser mount	University of Idaho machine shop, Moscow, ID 83844, USA	5/24/2012	1	$100

Total: $11,841 USD.

Low-cost LIDAR?

1st May

Yang, X., Li, R., Jablonski, A., Stovall, A., Kim, J., Yi, K., ... & Lerdau, M. (2023). Leaf angle as a leaf and canopy trait: Rejuvenating its role in ecology with new technology. *Ecology Letters*.

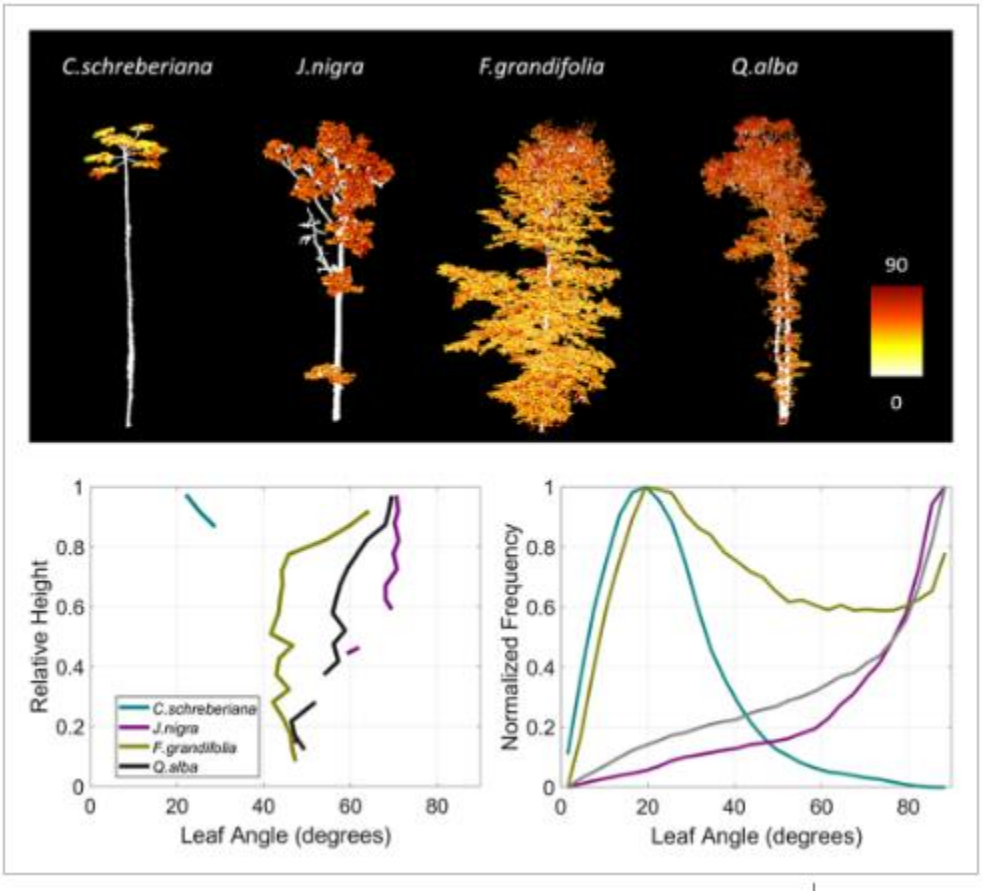

Nice review for leaf angle effect

4th April

Calders, K., Brede, B., Newnham, G., Culvenor, D., Armston, J., Bartholomeus, H., ... & Herold, M. (2023). StrucNet: a global network for automated vegetation structure monitoring. *Remote Sensing in Ecology and Conservation*.

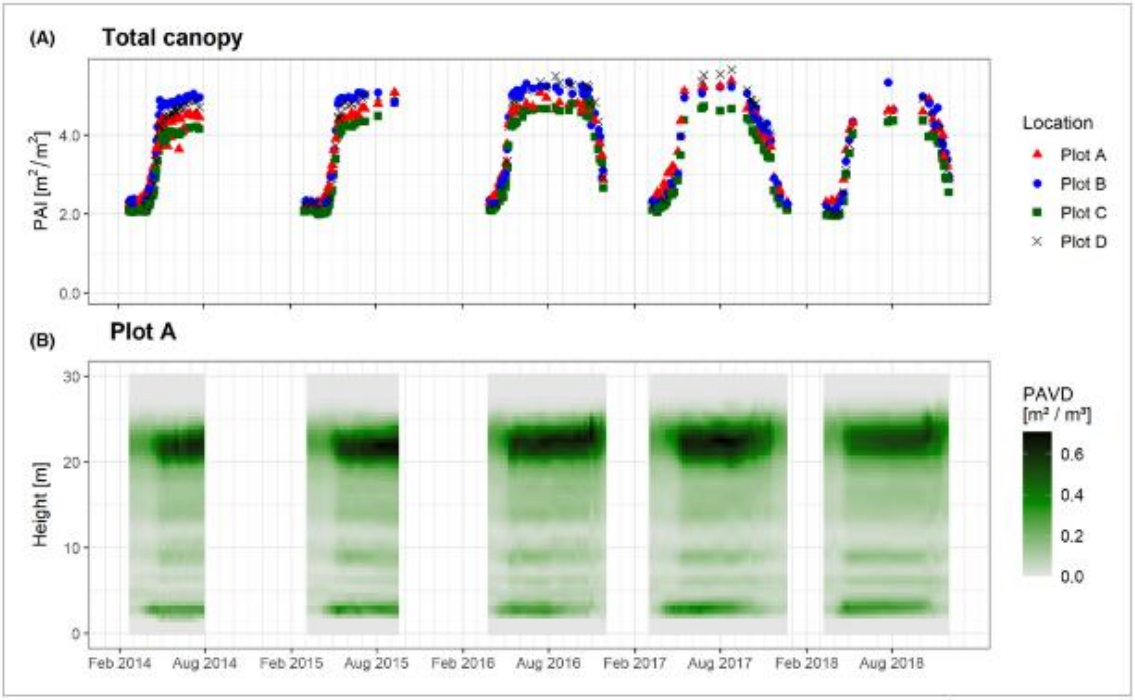

Figure 1

Open in figure viewer | PowerPoint

Five-year dynamics of forest structure for the four sampling locations in Dassenbos. Data were collected using the same measurement protocol and data analysis as described in Calders et al. (2015) using a zenith range of 35–70° for 184–186 (some scans were discarded for quality purposes) measurement days during the period from February 2014 to November 2018. Panel (A) represents total canopy plant area index (PAI) estimates derived from a terrestrial laser scanning (TLS) vertical plant profile. Panel (B) shows plant area volume density (PAVD) for each measurement at sampling location A.

Nice review for network

3rd April

Liu, L., Gudmundsson, L., Hauser, M., Qin, D., Li, S., & Seneviratne, S. I. (2020). Soil moisture dominates dryness stress on ecosystem production globally. *Nature communications*, *11*(1), 4892.

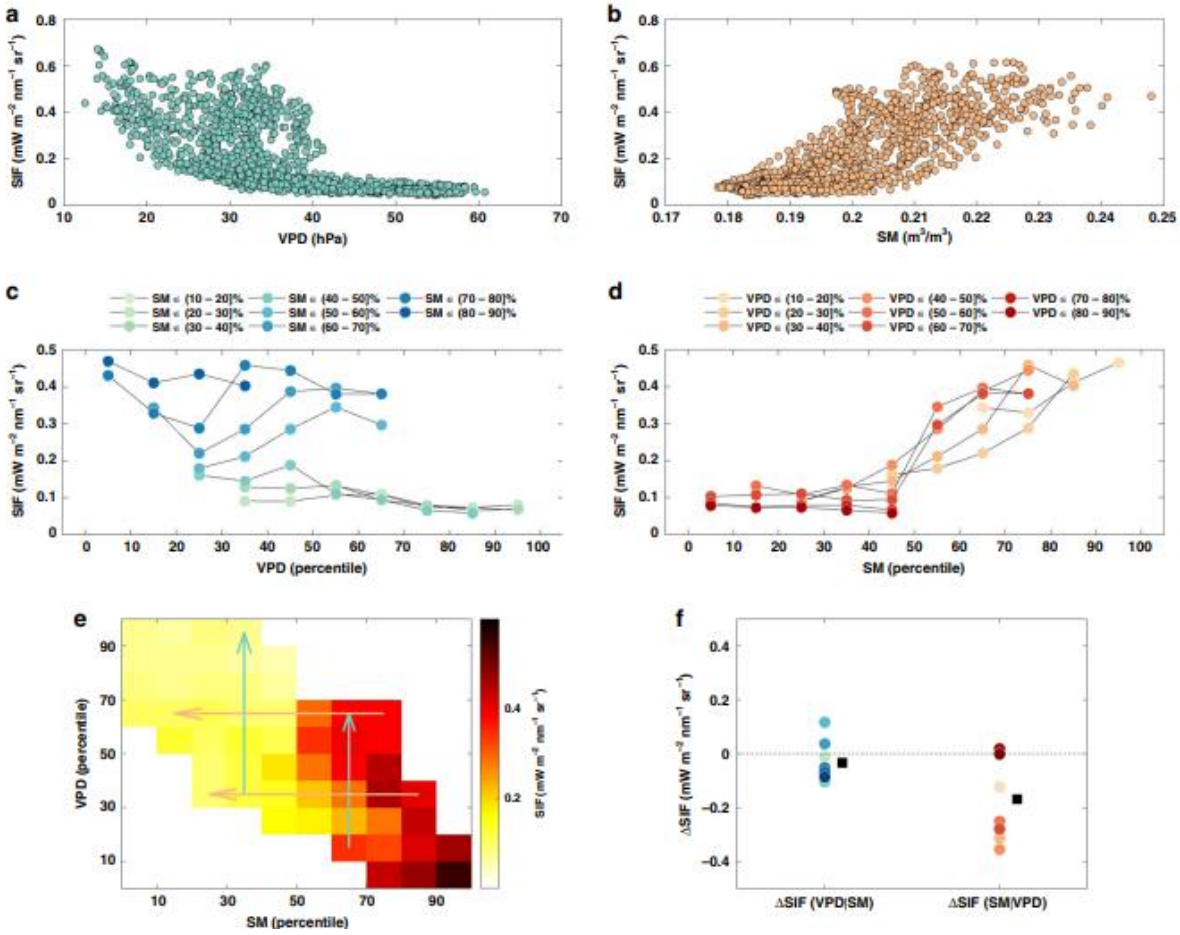

Is the VPD effect really less effective in reducing ChlF?

2nd April

Meng, F., Hong, S., Wang, J., Chen, A., Zhang, Y., Zhang, Y., ... & Piao, S. (2023). Climate change increases carbon allocation to leaves in early leaf green-up. *Ecology Letters*.

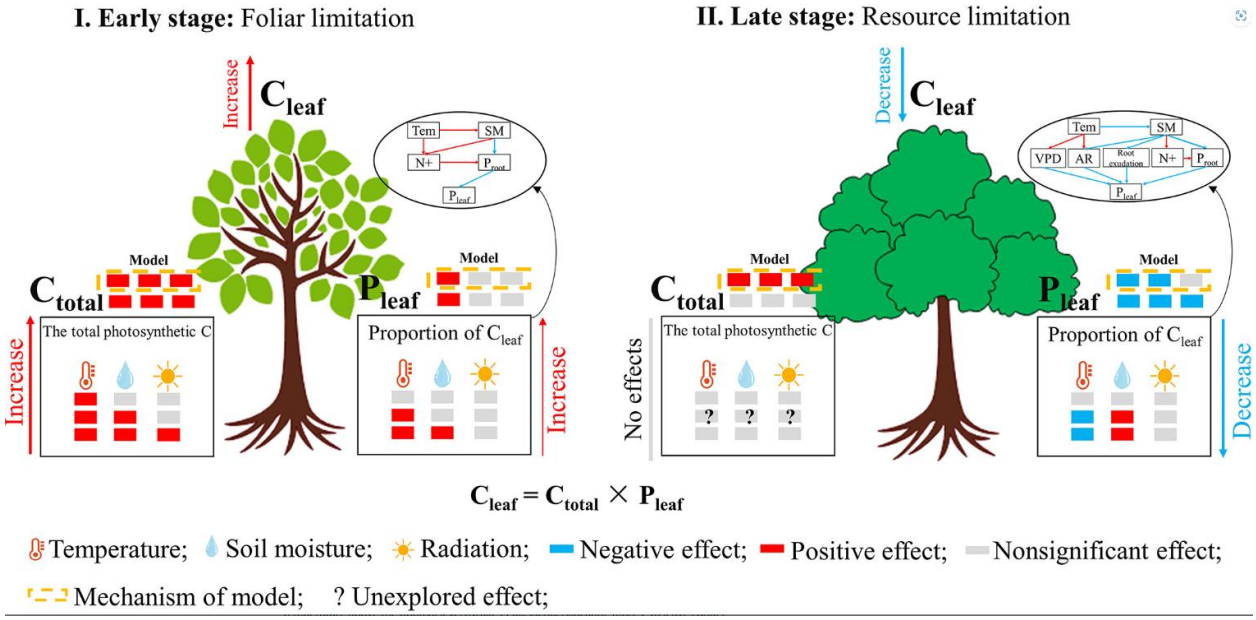

What are the implications of multi-layer study?

1st April

Zhang, Y., Fang, J., Smith, W. K., Wang, X., Gentine, P., Russell, S., ... & Zhou, S. (2023). Satellite solar-induced chlorophyll fluorescence tracks physiological drought stress development during 2020 southwest US drought. *Global Change Biology*.

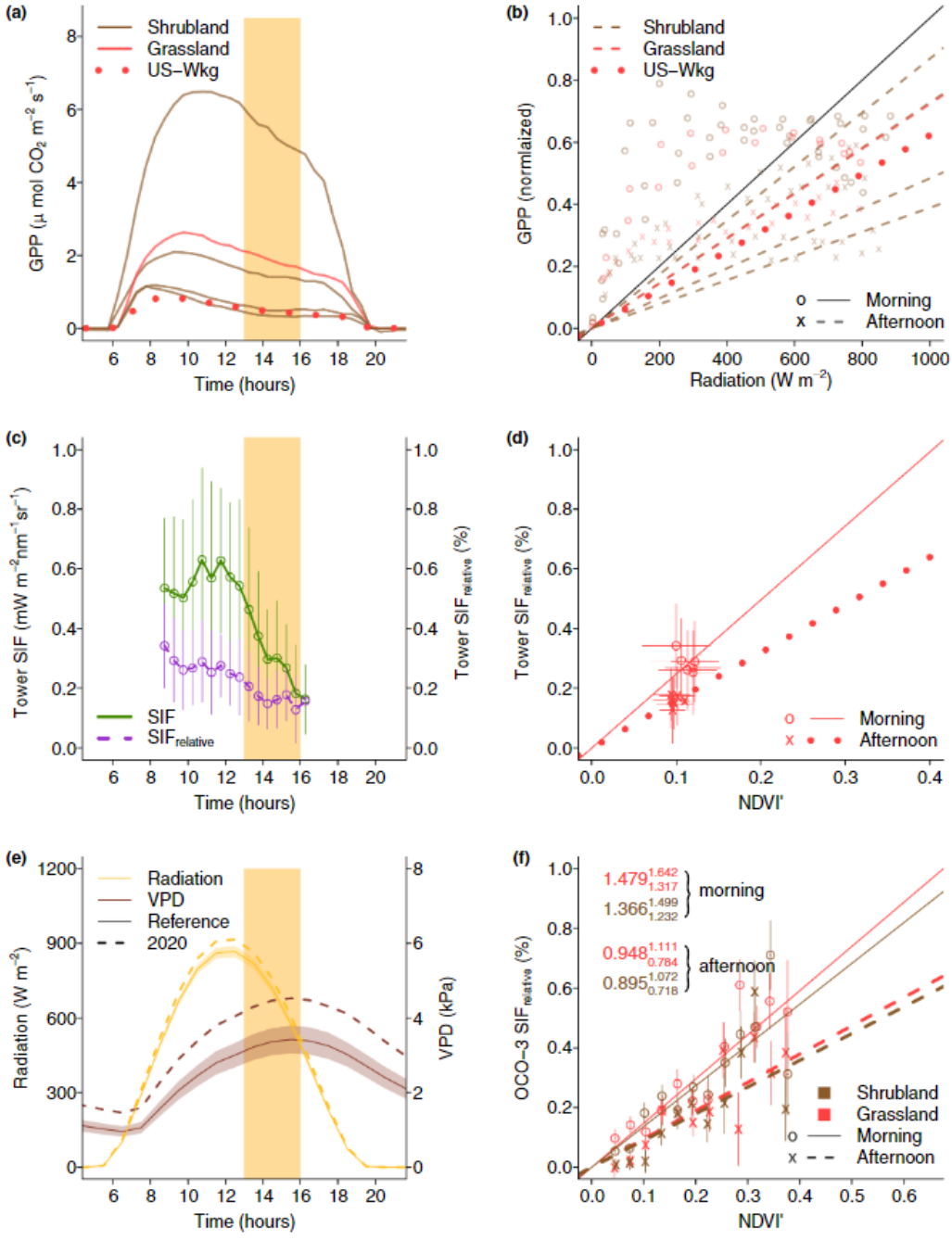

Diurnal variation of SIF, less related to structure?

3rd March

Zeng, Y., Badgley, G., Chen, M., Li, J., Anderegg, L. D., Kornfeld, A., ... & Berry, J. A. (2020). A radiative transfer model for solar induced fluorescence using spectral invariants theory. *Remote Sensing of Environment*, *240*, 111678.

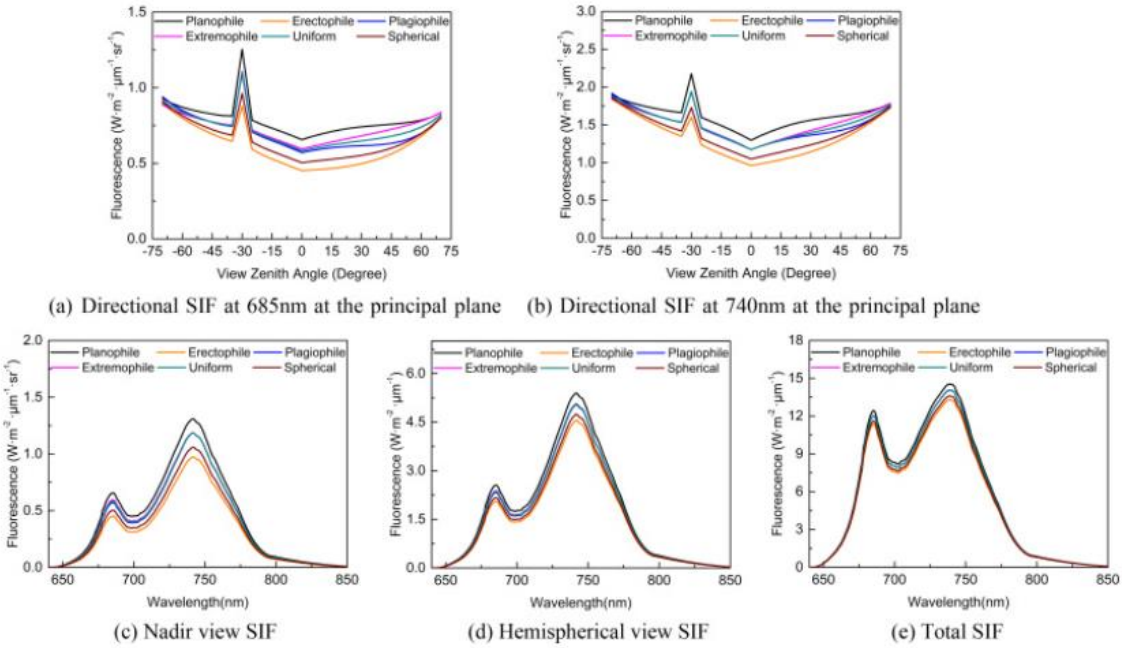

Download : Download high-res image (886KB)

Download : Download full-size image

Fig. 8. The directional observed SIF of Photosystem I+II at the principal plane at 685 nm (a) and at 740 nm (b), and the nadir view (c), hemispherical view (d) and total SIF (e) at different wavelengths by the FluorRTER model over 3D discontinuous canopies at different leaf angle distributions (LAD).

How does spectral invariant theory relate to SIF?

2nd March

Qiu, B., Ge, J., Guo, W., Pitman, A. J., & Mu, M. (2020). Responses of Australian dryland vegetation to the 2019 heat wave at a subdaily scale. *Geophysical Research Letters*, *47*(4), e2019GL086569.

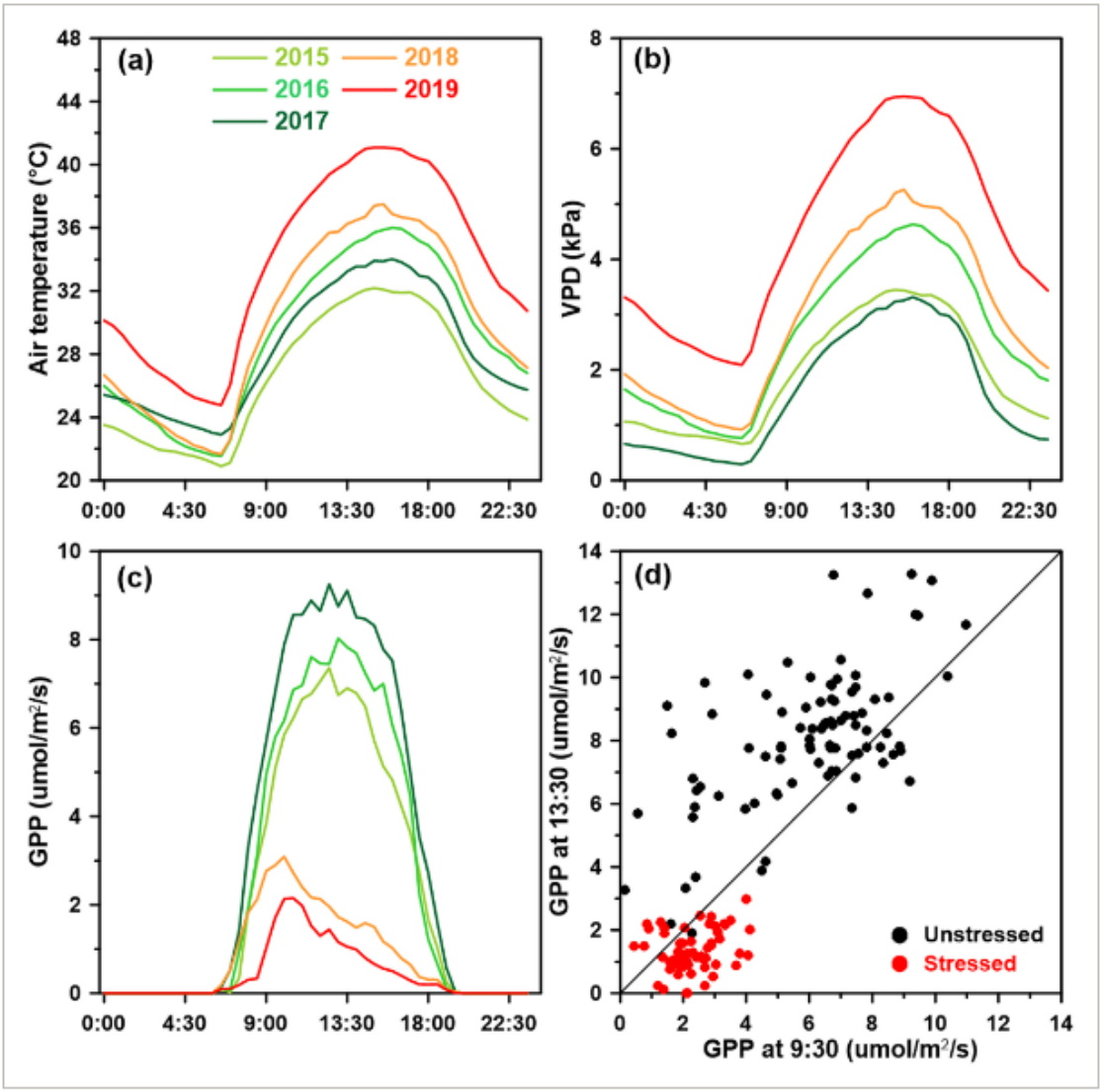

Figure 3

Open in figure viewer | PowerPoint

The mean diurnal (a) air temperature, (b) VPD, and (c) GPP measurements in January at the Alice Springs site, and (d) the scatterplot of January GPP at 9:30 a.m. and 1:30 p.m. from 2015 to 2019. The black and red dots are measured GPP under weakly stressed (2015–2017) and highly stressed (2018–2019) conditions.

Midday GPP depression

1st March

Yin, G., Verger, A., Descals, A., Filella, I., & Peñuelas, J. (2022). A broadband green-red vegetation index for monitoring gross primary production phenology. *Journal of Remote Sensing*.

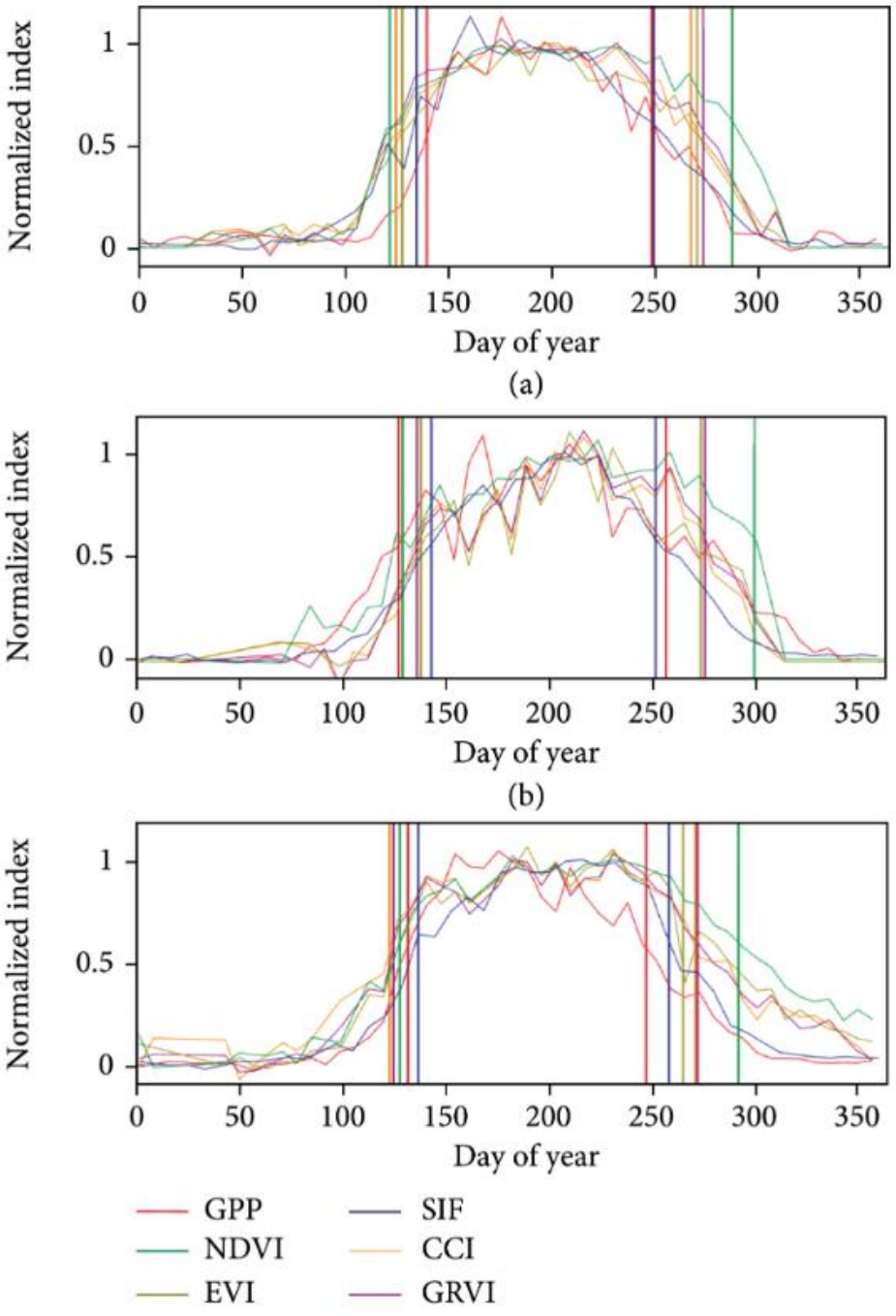

How is the SOS of the various VIs different?

4th Feb

Zhang, J., Xiao, J., Tong, X., Zhang, J., Meng, P., Li, J., ... & Yu, P. (2022). NIRv and SIF better estimate phenology than NDVI and EVI: Effects of spring and autumn phenology on ecosystem production of planted forests. *Agricultural and Forest Meteorology*, *315*, 108819.

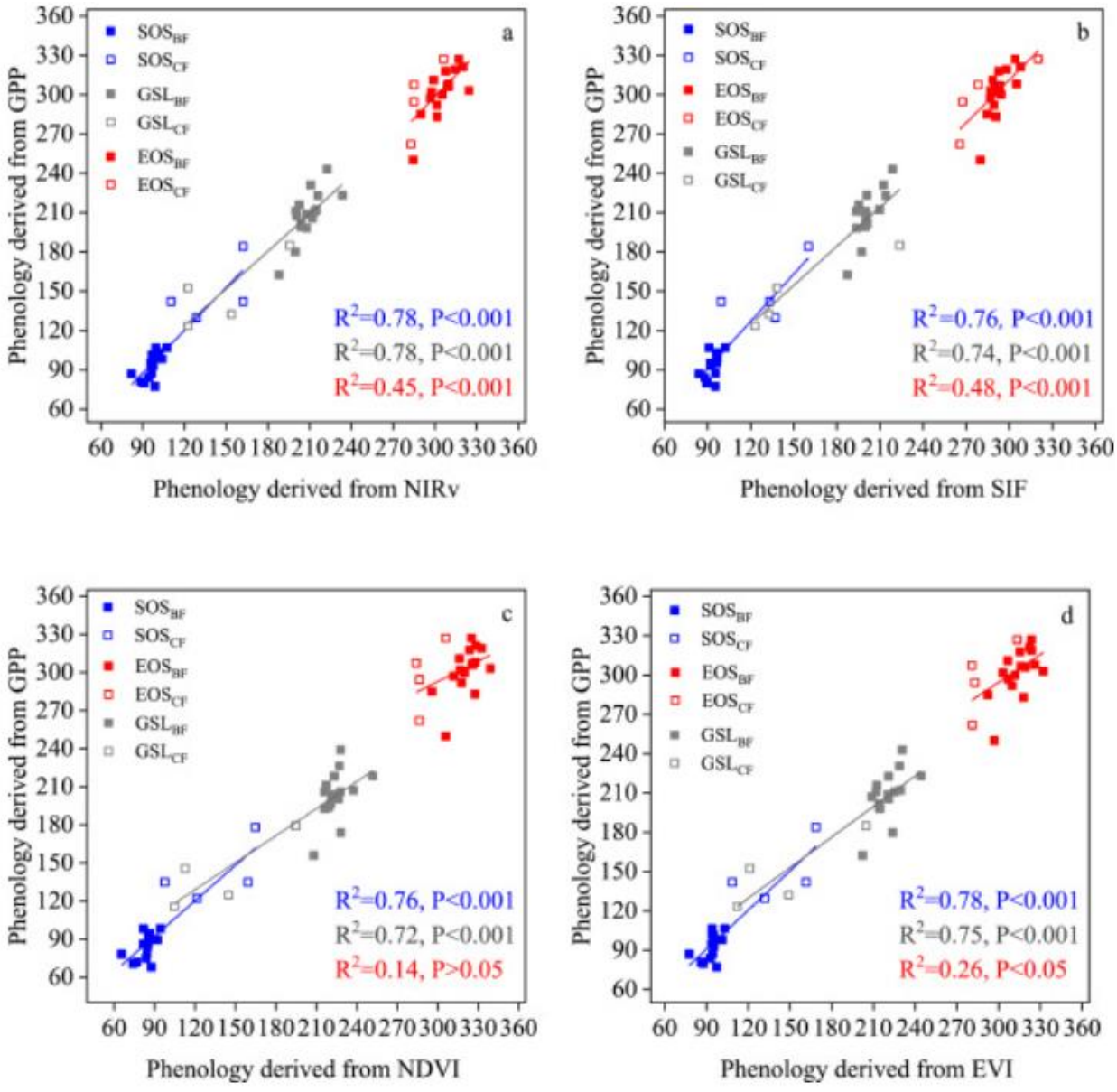

Do NIRv and NDVI track the phenology of GPP well?

3rd Feb

Li, S., Fang, H., & Zhang, Y. (2023). Determination of the Leaf Inclination Angle (LIA) through Field and Remote Sensing Methods: Current Status and Future Prospects. *Remote Sensing*, *15*(4), 946.

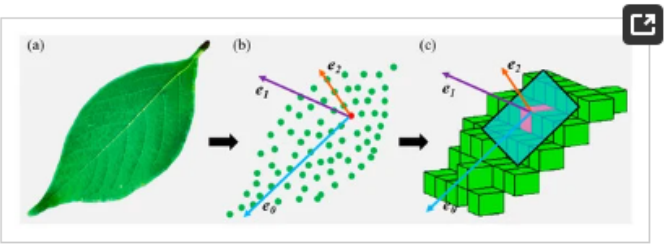

Figure 2. The LIA measurement of the leaf (**a**) based on the plane fitting of point clouds (**b**) and voxels (**c**). e_0, e_1, and e_2 denote the eigenvectors corresponding to the eigenvalues from the maximum to the minimum.

An alternative TLS method is based on the triangulation of 2D gridded point clouds [45,52] (Figure 3). The 3D point clouds (x, y, z) are projected on 2D spherical coordinates (θ, φ) encompassing zenith and azimuth angles from the TLS perspective according to the scan spaces (Figure 3a). Each point (i, j) is triangulated in the 2D gridded space by searching for and connecting neighboring hit points (Figure 3a). Once the triangulations are completed, the normal vectors of the triangles are computed in 3D space as the cross product of the two sides of the triangle, and the LIA is obtained accordingly (Figure 3c).

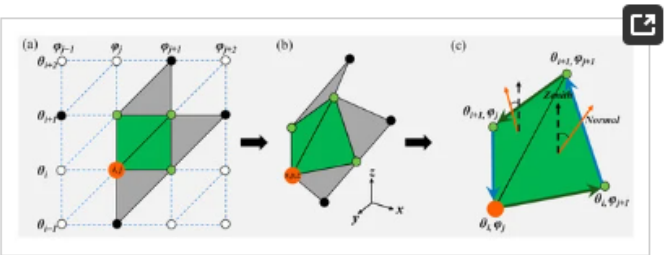

Figure 3. The schematic of point cloud triangulation in two-dimensional spherical coordinates (θ, φ) (**a**) and corresponding three-dimensional cartesian coordinates (x, y, z) (**b**). (**c**) depicts the computation of the normal vector and LIA by the cross-product of the two sides of the triangle (adapted from Bailey and Mahaffee [45]).

Nice review paper about the leaf angle calculation

2nd Feb

Kattenborn, T., Leitloff, J., Schiefer, F., & Hinz, S. (2021). Review on Convolutional Neural Networks (CNN) in vegetation remote sensing. *ISPRS journal of photogrammetry and remote sensing*, *173*, 24-49.

Despite such possibilities to decrease computation load, it has to be considered that projections or voxel representations of the point cloud will result in a loss of the original spatial detail. Therefore, it may be desirable to use end-to-end learning directly with the raw point cloud data as input. Using the raw point clouds instead of voxel or projections may be more computationally demanding but it can be assumed that ongoing developments in processing and algorithms will advance capabilities to harness point clouds directly. Another challenge is that point clouds are unordered sets of vectors (in contrast to elements in raster layers) and their analysis requires a spatial invariance with respect to rotations and translations. A well-known CNN architecture that considers these challenges is *PointNet*, which, hence, enables efficient end-to-end learning on point clouds. The foundation of *PointNet* are symmetric functions to ensure permutation invariance with regard to the unordered input and transforms the data into a canonical feature space to ensure spatial invariance. Even though *PointNet* or similar algorithms have been used comparatively rarely so far, the results are very promising: (Jin et al., 2020) applied *PointNet* to detect ground points under dense forest canopies and found greater accuracy than for traditional non-deep learning methods. Briechle et al. (2020) tested *PointNet* to classify temperate tree species in UAV LiDAR data and reported an overall accuracy of up to 90%. Bingxiao et al. (2020) and Windrim and Bryson (2020) used modified versions of *PointNet*, which besides point coordinates also considers the LiDAR return intensity, and demonstrated high accuracy in differentiating woody elements and foliage for multiple coniferous and deciduous tree species (up to 93–96% overall accuracy). The results of the aforementioned studies are especially remarkable, considering that this approach performs a classification at the highest possible detail, i.e. at the level of individual points.

What about machine learning in TLS data?

1st Feb

Campos, M. B., Litkey, P., Wang, Y., Chen, Y., Hyyti, H., Hyyppä, J., & Puttonen, E. (2021). A long-term terrestrial laser scanning measurement station to continuously monitor structural and phenological dynamics of boreal forest canopy. *Frontiers in Plant Science*, *11*, 606752.

FIGURE 1 | (A) the 30-m high measurement tower. The laser scanner is installed in a specially manufactured aluminum frame in the rear corner of the tower facing the test forest. **(B)** The winter view over the test forest next to the RIEGL VZ-2000i laser scanner in February 2020. **(C)** The summer view over the test forest in June 2020. The thick cable coming from the protective hood houses the data and power cables between the scanner, its external power unit and the measurement computer (not in figure).

Continuous canopy structure measurement by using LIDAR

4th Jan

Zhang, Z., Zhang, X., Porcar-Castell, A., Chen, J. M., Ju, W., Wu, L., ... & Zhang, Y. (2022). Sun-induced chlorophyll fluorescence is more strongly related to photosynthesis with hemispherical than nadir measurements: Evidence from field observations and model simulations. *Remote Sensing of Environment*, *279*, 113118.

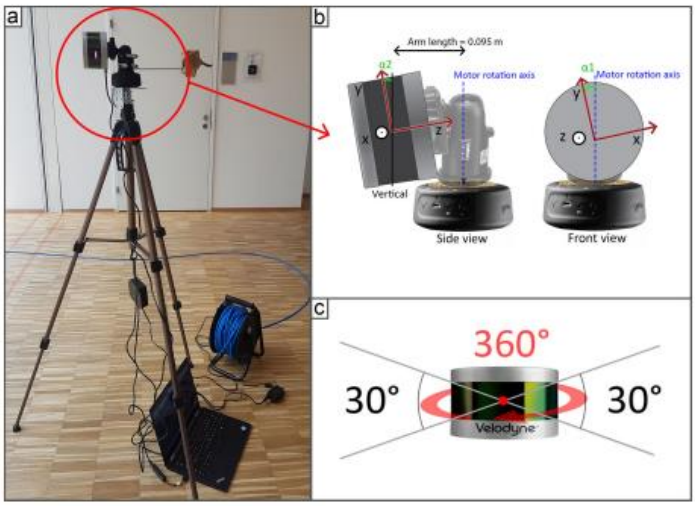

Figure 2. (a) Terrestrial lidar system (TLS); **(b)** two adjustments angles: collimation axis (α_1) and tilting axis (α_2) between the system and the rotation axis; **(c)** field of view of the VLP-16.

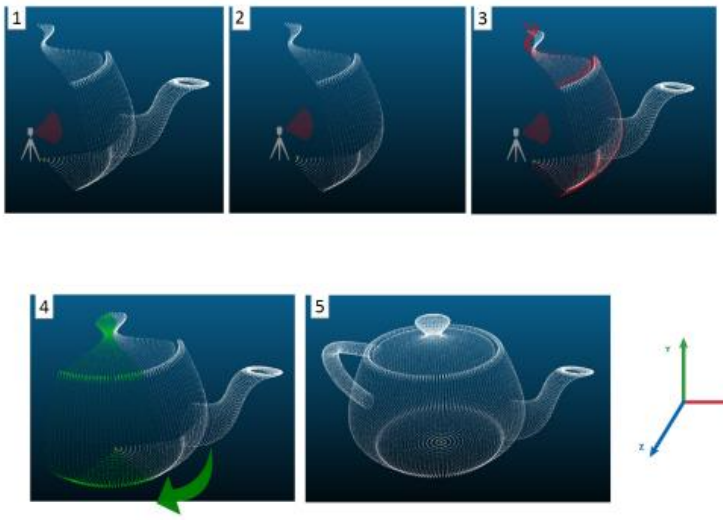

Figure 3. Steps to align the final. This is a synthetic example assuming that the lidar is located in the centre of the teapot point cloud.

Idea for Low-cost LIDAR system

3rd Jan

Zhang, Z., Zhang, X., Porcar-Castell, A., Chen, J. M., Ju, W., Wu, L., ... & Zhang, Y. (2022). Sun-induced chlorophyll fluorescence is more strongly related to photosynthesis with hemispherical than nadir measurements: Evidence from field observations and model simulations. *Remote Sensing of Environment*, *279*, 113118.

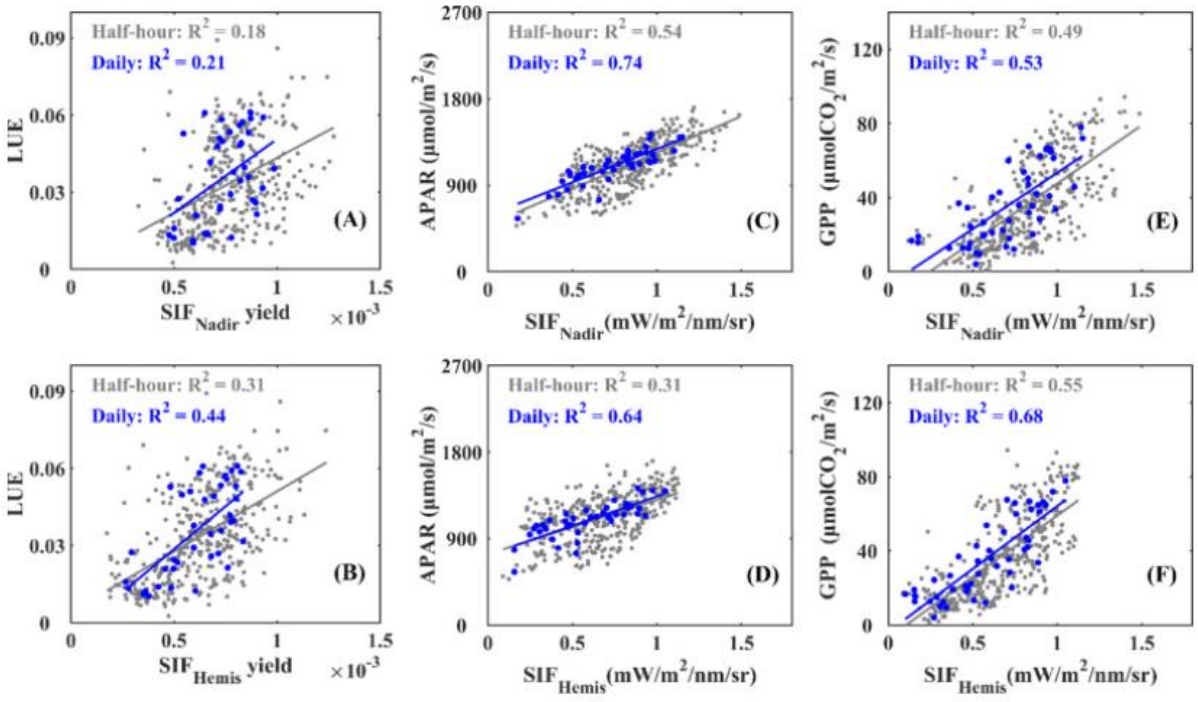

Download : Download high-res image (795KB) Download : Download full-size image

Fig. 6. Scatter plots and linear regressions (y = a × x + b) between the LUE and (A) SIF_{Nadir} yield and (B) SIF_{Hemis} yield for half-hourly data (gray circle) and daily data (blue circle). (C—D) Similar to (A-B) but for relationships between the APAR and SIF. (E-F) Similar to (A-B) but for relationships between the GPP and SIF. All regressions were statistically significant ($p < 0.05$). (For interpretation of the references to colour in this figure legend, the reader is referred to the web version of this article.)

Conical-based SIF VS hemispherical-based SIF with GPP

2nd Jan

Wu, Y., Zhang, Z., Zhang, X., Wu, L., & Zhang, Y. How do sky conditions affect the relationships between ground-based solar-induced chlorophyll fluorescence and gross primary productivity across different plant types?. *Journal of Geophysical Research: Biogeosciences*, e2022JG006865.

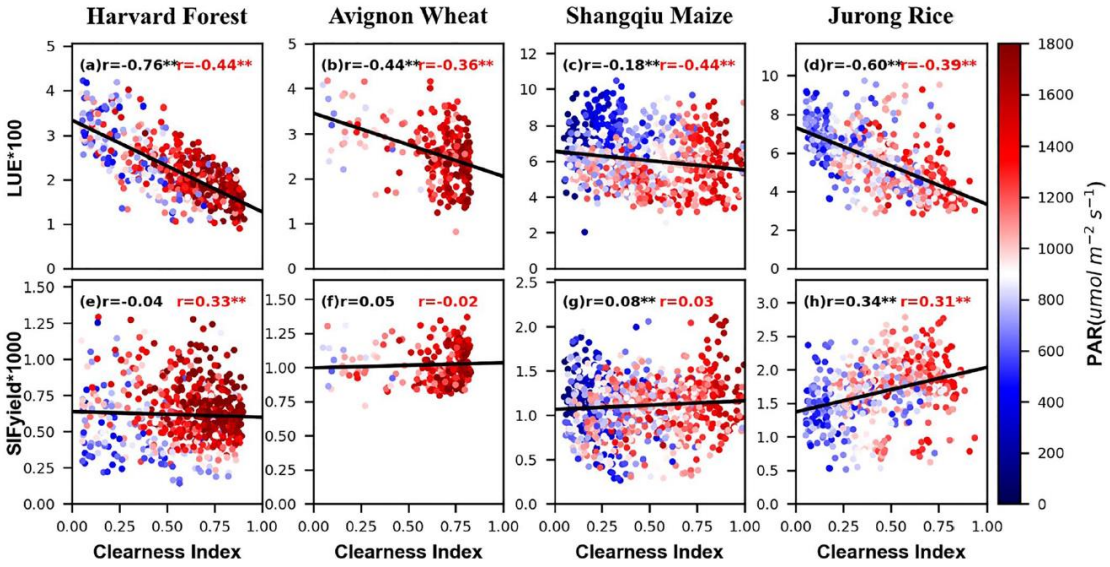

Figure 4. Responses of light use efficiency (LUE) (μmol CO_2/μmol photons) and SIF_{yield} (μmol photons@760 nm/μmol photons) to clearness index (CI) for (a) Harvard Forest, (b) Avignon Wheat, (c) Shangqiu Maize, and (d) Jurong Rice. The correlation coefficients (r) of LUE (or SIF_{yield}) with CI and photosynthetic active radiation were shown in black and in red, respectively. ** denote the statistical significance $p < 0.05$.

SIF-GPP relationship over different sky conditions.

1st Jan

Amarnath, K., Bennett, D. I., Schneider, A. R., & Fleming, G. R. (2016). Multiscale model of light harvesting by photosystem II in plants. *Proceedings of the National Academy of Sciences*, *113*(5), 1156-1161.

Fig. 1.

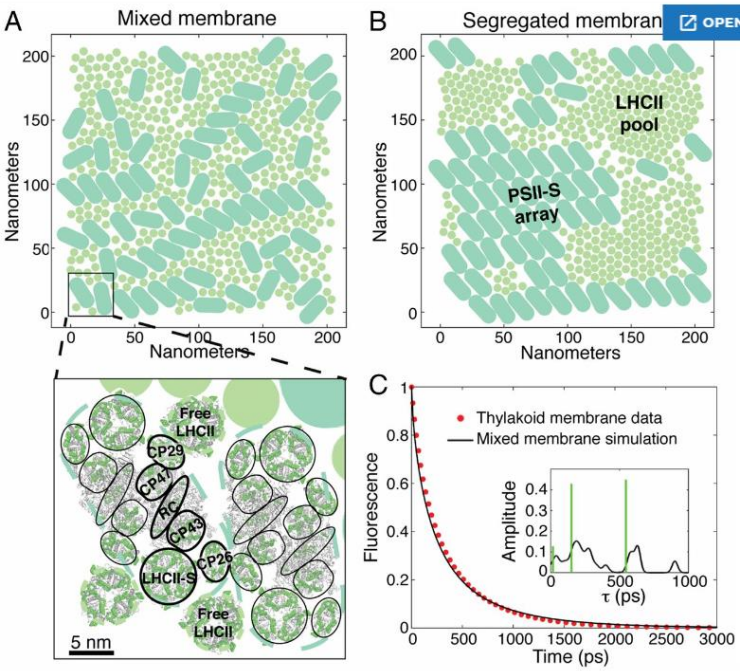

Recent advances have established structure–function relationships within individual pigment–protein complexes, but not how these relationships affect the functioning of the dynamic PSII (grana) membrane (10). Electron microscopy and fitting of atomic resolution structures (11) place the pigment–protein complexes in the grana membrane in close proximity, enabling long-range transport. Indeed, connectivity of excitation between different PSII reaction centers has been discussed since 1964 (12), suggesting that the functional unit for PSII must involve a large area of the membrane. Two limiting cases have been used to model PSII light harvesting: The lake model assumes perfect connectivity between reaction centers across the membrane; alternatively, the membrane can be described as a collection of disconnected "puddles" of pigments that each contain one reaction center (1, 13). At present, however, resolving the spatiotemporal dynamics within the grana membrane on the relevant length (tens to hundreds of nanometers) and time (1 ps to 1 ns) scales experimentally is not possible. Structure-based modeling of the grana membrane, however, can access this wide range of length and time scales.

What is the difference between puddle and lake model
